Article

Phase Distribution of Gas–Liquid Slug–Annular Flow in Horizontal Parallel Micro-Channels

Yanchu Liu [1], Siqiang Jiang [2] and Shuangfeng Wang [2,*]

1   Shenzhen Key Laboratory of Soft Mechanics & Smart Manufacturing, Department of Mechanics and Aerospace Engineering, Southern University of Science and Technology (SUSTech), Shenzhen 518055, China; liuyc@sustech.edu.cn
2   Key Lab of Heat Transfer Enhancement and Energy Conservation of Ministry of Education, School of Chemistry and Chemical Engineering, South China University of Technology, Guangzhou 510640, China; 18819466580@163.com
*   Correspondence: sfwang@scut.edu.cn; Tel.: +86-20-22236929

Abstract: As a transitional flow pattern, slug–annular flow occurs over a wide range of operating conditions in micro-channels while its distribution in parallel micro-channels has not been well characterized. Herein, we conducted an experiment to study the phase distribution of slug–annular flow in parallel micro-channels. The test section consists of a header with a diameter of 0.48 mm and six branch channels with a diameter of 0.40 mm. Nitrogen and 0.03 wt% sodium dodecyl sulfate (SDS) solution were used as the test fluids. It was found that the phase distribution of the slug–annular flow was unstable and the duration of the varying process showed regularity with different inlet conditions. Increasing the liquid superficial velocity facilitated the liquid phase to flow into channels at the fore part of the header, while the channels at the rear part of the header were more supplied with liquid as the gas superficial velocity, volume fraction of gas, and volume flow rate increased. Furthermore, the results indicated that the channels located at the rear part of the header experienced a pronounced enhancement in the supply of both the liquid and gas phases, with the spacing between the branches increasing. A predictive correlation was formulated to ascertain the distribution of the liquid phase within slug–annular flow across parallel micro-channels.

Keywords: slug–annular flow; two-phase; phase distribution; visualization; parallel micro-channels; branch spacing

1. Introduction

Parallel micro-channels, functioning as fluid distributors to segregate a singular inlet stream into multiple branches, are ubiquitously employed across a vast array of industrial apparatus, including reactors [1], mixers [2], and heat exchangers [3], among others. Notably, the fluidic properties undergo significant alterations when the system dimensions are scaled down to the micro-scale, defined by a diameter range of 1 μm to 1000 μm [4]. This diminution engenders a substantial increase in the specific surface-to-volume ratio and the contact area, markedly enhancing the heat and mass transfer processes [5]. Consequently, parallel micro-channels find extensive applications in various domains, such as mobile air-conditioning systems, automotive technologies, and residential micro-channel condensers. However, the phase distribution within the branched channels frequently exhibits non-uniformity due to phase separation phenomena, markedly impacting the efficiency of downstream devices, such as the diminished thermal and hydraulic performance in compact heat exchanger evaporators, the emergence of dry-out zones in evaporators, and the formation of zones with excessive liquid accumulation in condensers [6–8]. Given these factors, a thorough study of phase distribution in parallel channels is crucial to improve phase uniformity and optimize equipment performance.

Recent research on adiabatic gas–liquid two-phase flow in parallel channels has primarily focused on three factors affecting phase distribution: operational conditions (like flow velocities, patterns, and system orientation), geometric parameters (such as header dimensions and channel layout), and fluid properties [9,10]. A significant portion of these studies has predominantly focused on the impact of operational conditions. For instance, Osakabe et al. [11] observed that the flow rate to the initial channel surged as the rates to subsequent channels diminished with an increase in the air flow rate at the header's inlet. Conversely, as the air velocity further escalated, the distribution rate to the initial branch gradually declined, while the rates to other channels tended to rise. Kim and Sin [12] noted that an increase in the mass flux or quality generally led to enhanced water distribution towards the header's rear, with air distribution patterns typically exhibiting an inverse relationship to the water distribution. Marchitto et al. [10] highlighted that an elevated inlet gas flow rate could enhance the uniformity of the gas distribution but detrimentally affect the liquid phase distribution's homogeneity. Furthermore, Ahmad et al. [13], Dario et al. [14], and Liu et al. [15] conducted experimental investigations to examine the influence of the orientation of headers and channels, demonstrating that the two-phase flow distribution among channels was significantly influenced by the orientation, particularly when gravitational forces impacted the flow behavior within the header.

Some studies have examined how fluid properties and geometry influence phase distribution in parallel channels. Zhang et al. [16] observed notable differences when testing with air, water, and R-134a. Kim et al. [17,18] reported that air–water mixtures led to a more even distribution than air–R-134a. Chen et al. [19] indicated that higher surface tension fluids might block some branches. Zou and Hrnjak [20] found R245fa to have the most uniform distribution among various fluids. Geometrically, Horiki et al. [21] saw more uneven distributions in rectangular versus square headers, while Vist and Pettersen [22] linked smaller header diameters to better phase uniformity. Marchitto et al. [10] highlighted the dual effects of reducing the channel diameter on the gas and liquid distribution. Studies by Lee and Lee [23], Kim and Sin [12], Kim and Han [24], and Marchitto et al. [25] showed that adjusting the channel protrusion depth could improve the homogeneity. Hwang [26] and Lee's [27] work on branch spacing in T-junctions found that closer branches led to less liquid removal downstream, not accounting for end plate effects.

These findings provide valuable insights into phase distribution research within parallel channels, primarily focusing on systems connected to headers of a mini (1 mm to 5 mm) or macro-scale (diameters greater than 5 mm). However, as system dimensions are reduced to the micro-scale (1 μm to 1000 μm), the influence of various factors shifts [28]. At this scale, surface tension plays a pivotal role in slug and slug–annular flows (where the Capillary number approaches zero), whereas inertial forces gain prominence in slug–annular flows (with the Weber number exceeding one) [29]. The significance of gravity and buoyancy diminishes with a reduction in the Bond number. Additionally, Triplett et al. [4] demonstrated the non-negligible impact of viscous and surface forces in channels with hydraulic diameters smaller than the Laplace constant, defined as $\lambda = [\sigma/g(\rho_l - \rho_g)]^{1/2}$. Consequently, micro-scale channels exhibit distinct behaviors; for example, stratified flow is not present, and dispersed bubble flow becomes uncommon, with bubbly flow typically manifesting as a series of spherical bubbles smaller than the channel's diameter [30,31].

Slug–annular flow, spanning a broad spectrum of operational conditions in micro-channels, is situated between the slug and annular flow transition lines on flow regime maps [4,32]. Despite its significance, particularly in chemical engineering and heat transfer applications where it promotes enhanced throughput and efficiency, especially in phase-changing systems, slug–annular flow in parallel micro-channels remains underexplored [29]. This study focuses on the slug–annular flow regime at the inlet, examining the impact of the inlet conditions and branch spacing on the phase distribution. The evolution of slug–annular flow distribution was meticulously analyzed by tracking data variations over time, highlighting the unique stabilization processes and consistent duration patterns under varying inlet conditions.

2. Experiments

2.1. Experimental Apparatus and Procedure

Figure 1a presents a detailed schematic of the experimental setup. Nitrogen gas was sourced from a tank, with its flow rate meticulously regulated by a mass flow controller (MFC, CMQ-V9500, Azbil Corporation, Tokyo, Japan). Liquid delivery was achieved through two precision syringe pumps (LSP02-1B, Longerpump Corporation, Baoding, China), allowing for precise control over the liquid flow rates. These gas and liquid streams were combined in a micro-cross mixer (dimensions 0.6 mm by 0.4 mm) to create the two-phase flow. To ensure the flow was fully developed, the mixer's downstream outlet was linked to the header of the test section via a channel, the length of which was 100 times its diameter. Upon exiting the test section, the two-phase flow was directed into six separate gas–liquid separators. The flow rate of liquid from each branch channel was determined by measuring the weight increase of the discharged liquid over a set time period using an electronic scale (BSM-120.4, Shanghai Zhuojing Electronic Technology Co., Ltd., Shanghai, China). The gas flow rates at the outlets were ascertained using bubble meters. The flow behavior within the transparent micro-channels was visualized using a high-speed camera (Phantom VEO 410L, Vision Research Corporation, Birmingham, Alabama, USA) operating at 10,068 frames per second with a resolution of 1024 × 512 pixels.
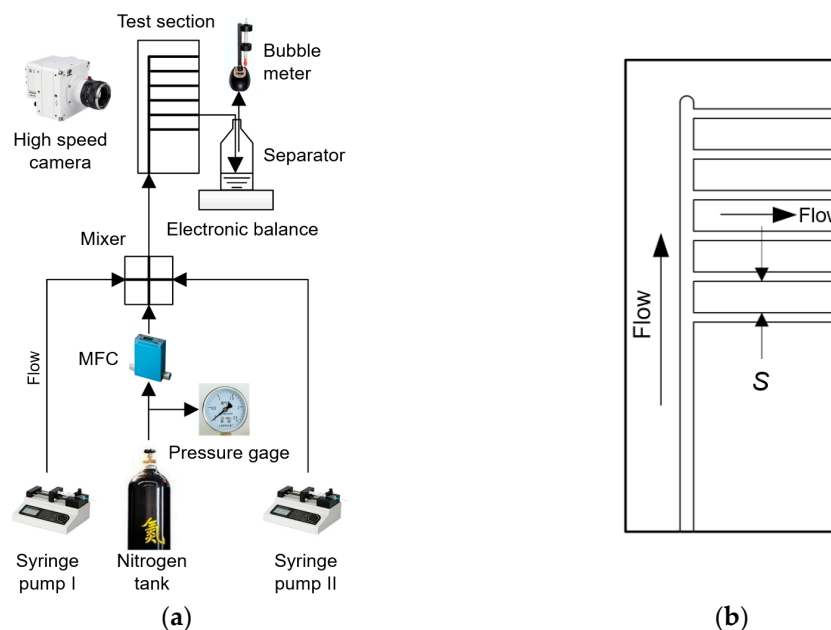

Figure 1. (**a**) Schematic diagram of the experimental apparatus (the arrows show the flow direction); (**b**) Configuration of the test sections.

The test section consisted of six parallel micro-channels linked to a shared header, all constructed from transparent polymethyl methacrylate (PMMA) to facilitate observation. The header featured a rectangular cross-section of 0.6 mm by 0.4 mm, while the channels had dimensions of 0.4 mm by 0.4 mm each. Figure 1b illustrates the layout of the test section. To examine the influence of branch spacing, the gaps between adjacent micro-channels were set at 0.8 mm, 4 mm, and 12 mm. Each channel extended 60 mm in length, with the header protruding an additional 0.6 mm beyond the final channel to buffer the flow.

An analysis to quantify the uncertainty in the measured variables was conducted. The uncertainty associated with experimental conditions derives from equipment inaccuracies inherent in instruments. The precision of the gas flow rate, regulated by the mass flow controller (MFC), was within ±1.0%. The liquid flow rate, determined by the syringe pump, had an accuracy of ±0.5%. The uncertainty linked to the outlet liquid flow rates, as measured by electronic balances, was confined to ±0.2%. To ensure the reliability of the

experimental outcomes, comprehensive mass balances for both gas and liquid phases were verified, and any data deviating from the mass balance by more than $\pm6.5\%$ were excluded from consideration.

2.2. Experimental Conditions and Calculations

The experiments were conducted under standard atmospheric pressure and at ambient temperature conditions. Nitrogen served as the gas phase while a 0.03 wt% SDS solution was employed as the liquid phase. The physical properties of these working fluids are detailed in Table 1. To investigate the distribution patterns of the two-phase slug–annular flow, four distinct experimental series were undertaken within the test section, where the spacing-to-diameter ratio (S/d) was set to 10, encompassing a total of eleven experimental cases. The J_g (inlet gas superficial velocity), J_l (inlet liquid superficial velocity), Q (volume flow rate) and x_g (volume fraction of gas) of all the cases are summarized in Table 2. Case 4 and case 10 were selected as the inlet conditions to explore the effect of branch spacing.

Table 1. Properties of the working fluids (at ambient temperature).

	ρ (kg/m^3)	σ (mN/m)
Liquid (0.03 wt% SDS solution)	997.35	29.2
Gas (nitrogen)	1.25	—

Table 2. Inlet conditions and the corresponding parameters.

Series	Case	J_g (m/s)	J_l (m/s)	Q (mL/s)	x_g
	1		0.12	1.73	0.98
a	2	7.08	0.18	1.74	0.98
	3		0.21	1.75	0.97
	4		0.30	1.77	0.96
	5	5.97		1.48	0.97
b	2	7.08	0.18	1.74	0.98
	6	9.03		2.21	0.98
	7	12.08		2.94	0.99
	2	7.08	0.18		0.98
c	8	6.95	0.28	1.74	0.96
	9	6.81	0.42		0.94
	2	7.08	0.18	1.74	
d	10	9.03	0.23	2.22	0.98
	11	12.08	0.31	2.97	

3. Results and Discussion

The characterization of two-phase flow patterns often involves the use of various dimensionless numbers that reflect the comparative significance of forces influencing flow dynamics, including inertia, viscous forces, and surface tension. Among these, the Reynolds number (Re) quantifies the inertia-to-viscous force ratio:

$$\mathrm{Re}_{k,in} = \frac{\rho_k (J_g + J_l) D_h}{\mu_k}, \tag{1}$$

and the Weber number (We) assesses the inertia-to-surface tension ratio:

$$\mathrm{We}_{k,in} = \frac{\rho_k (J_g + J_l)^2 D_h}{\sigma_k}. \tag{2}$$

In the context of this study, the Reynolds number for both the liquid and gas phases ranged from 92 to 324 and 279 to 566, respectively, indicating that the two-phase flow

regime was laminar. Meanwhile, the Weber number for the liquid and gas phases spanned from 0.33 to 4.06 and 1.02 to 4.17, respectively.

3.1. Inlet Flow Pattern

In this study, the inlet flow patterns were visually inspected under all the experimental conditions. Three distinct sub-patterns within the slug–annular flow regime were identified: liquid bridge, wavy liquid film, and smooth liquid film, as depicted in Figure 2a. To corroborate the flow patterns observed during the experiments, the experimental data were mapped onto existing flow pattern diagrams from the works of Chung and Kawaji [31], Triplett et al. [4], and Liu and Wang [33], as illustrated in Figure 2b. These reference maps were originally developed for channels with diameters closely resembling those used in this study, specifically 0.25 mm, 1.09 mm, and 0.48 mm.
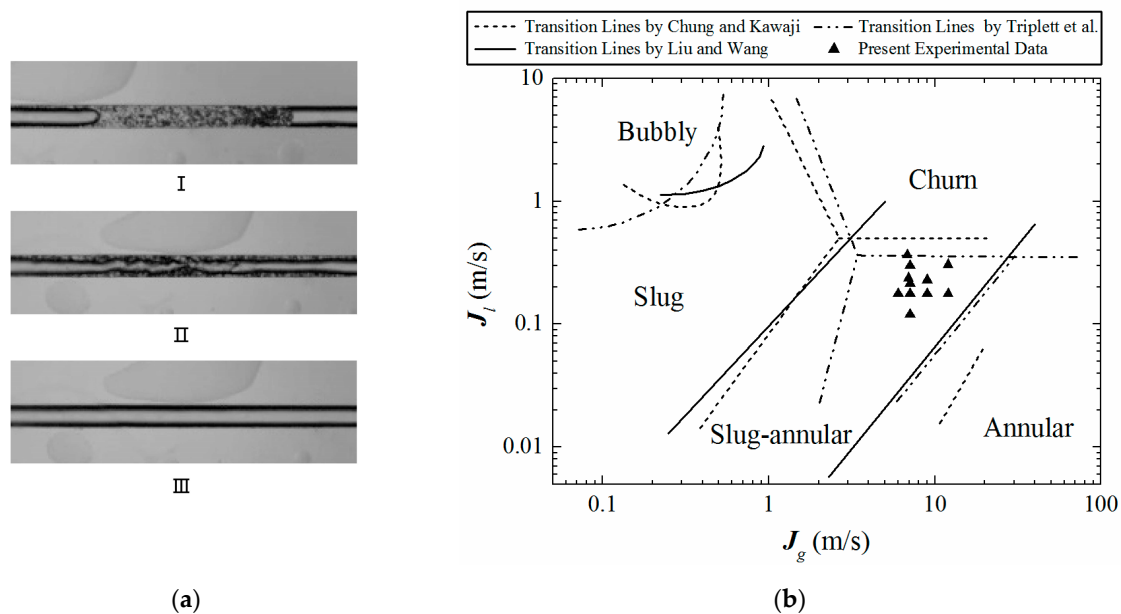

(a) **(b)**

Figure 2. (**a**) Typical three kinds of sub-patterns of slug–annular flow: I. liquid bridge; II. wavy liquid film; III. smooth liquid film; (**b**) Comparison of flow regime maps of present work with Chung and Kawaji [31], Triplett et al. [4], and Liu and Wang [33] (0.25, 1.09, and 0.48 mm hydraulic diameter, respectively). "▲" present experimental data.

3.2. Varying of Flow Distribution in Parallel Micro-Channels

The varying process of the flow distribution among the branch channels in case 3 (J_g = 7.08 m/s, J_l = 0.21 m/s) was plotted in Figure 3a to illustrate the representative distribution characteristics of slug–annular flow. The abscissa of Figure 3a represents the time from the two-phase flow entering the test section and the ordinate represents the mass fraction of the gas and liquid separated out through each channel, denoted as $F_{g,i}$ and $F_{l,i}$. Figure 3b shows the corresponding flow structures in the header at three different times and the typical flow behavior of a liquid bridge in a period.

The liquid tends to highly feed channel #5 and badly feed other channels in the beginning (t_1), while the gas tends to highly supply channel #4 and moderately feed channels #3 and #5. The mass fraction of the liquid phase in channel #5 decreases rapidly as the liquid mass fraction in channel #4 increases over time. Meanwhile, the liquid phase mass fractions in channels #2 and #3 increase slightly when there is a minor reduction of the liquid mass fraction in channels #1 and #6. As for the gas phase, the gas mass fractions of channels #4 and #5 decrease while more gas phase flows into channels #2 and #3 during t_1 to t_3. From t_3, the distributions of both liquid and gas eventually move into the stable region, in which the liquid phase highly feeds channel #4 and most gas phase tends to flow into channels #3 and #4.
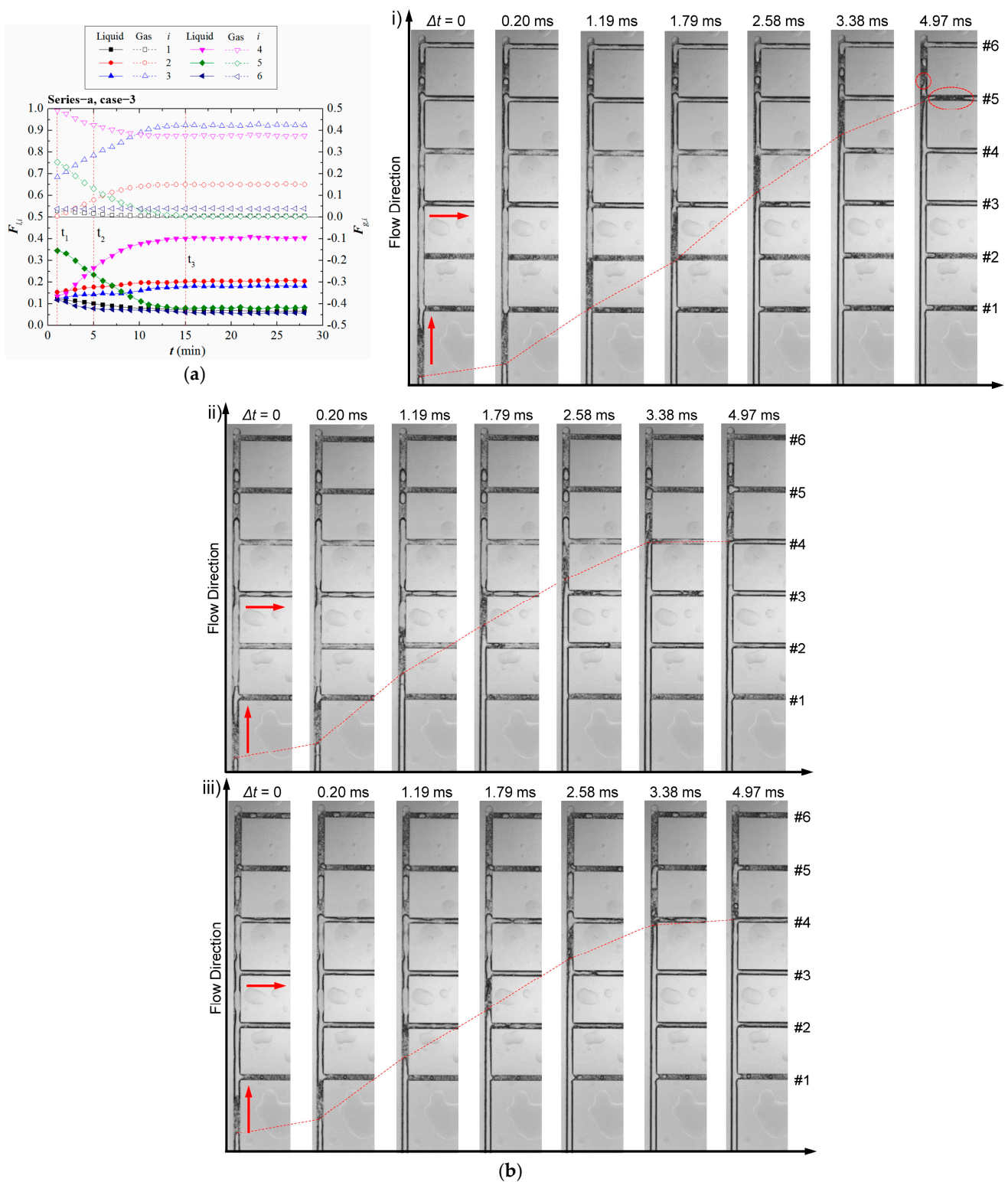
Figure 3. The process of varying of the flow distribution in parallel channels and the corresponding flow structures in the header at different times and the typical flow behavior of a liquid bridge (red dotted line) in a period in case 3 (J_l = 0.21 m/s, J_g = 7.08 m/s). #1–6 are the channel numbers starting from the fluid inlet direction and the red arrows show the flow direction in the channels. (**a**) The process of the varying of flow distribution in parallel channels in case 3 (J_l = 0.21 m/s, J_g = 7.08 m/s); (**b**) The corresponding flow structures in header and the typical flow behavior of a liquid bridge in a period: at t_1 = 1 min (i), 5 min (ii), and 15 min (iii).

The phase distribution results at different times can be explained as follows. At the beginning, when a liquid bridge enters the test section, it separates at each junction from channel #1 to #5 as the two-phase flow proceeds along the downstream direction, and then the last part of the liquid bridge stays at the rear header, waiting for another liquid bridge to push it into the channel #6, as shown in Figure 3b(i). Most of the liquid is taken off by channel #5 due to the large momentum flux of the liquid phase as well as the liquid pooling in the header between channel #5 and #6. Moreover, the large quantity of liquid increases the pressure drop in channel #5; therefore, most of the gas tends to flow into channel #4 instead of channel #5. As time goes on, when $t_2 = 5$ min, the amount of liquid staying in the header grows and the liquid column in the header becomes longer and longer, thus covering channel #5. As a result, the channels in the middle part of the header are more and more supplied with liquid, particularly channel #4, while channel #5 tends to be badly fed. Furthermore, the gas phase decreases in channel #4 and increases in channel #3 in the meantime, owing to the increase in the liquid mass fraction in channel #4. Finally ($t_3 = 15$ min), the liquid column in the header is long enough to cover the header from channel #4 to #6. Then, channel #4 replaces channel #5 and most of the liquid flows into it as most of the gas flows into channel #3. For the slug–annular flow, because of the irregular emergence of the liquid bridge, wavy liquid film, and smooth liquid film as time goes on, it is easy for the liquid to pool in the rear part of the header and the liquid flow to be sluggish in the channels at that part of the header; thus, the flow distribution varies with time.

Figure 4 shows the effect of the inlet conditions on the duration (t) of the flow distribution varying. It can be seen from the figure that it takes less time for the distribution to be stable with an increase in the inlet liquid superficial velocity, the gas superficial velocity, and the volume flow rate. In addition, the decrease in the volume fraction of gas can shorten the unstable time. This means the increase in the liquid superficial velocity plays the main role in shortening the unstable time, while the increase in the gas superficial velocity will matter when the liquid remains unchanged. This is because when the inlet liquid and gas velocity increase, more liquid and gas are delivered into the test section and the balance of the pressure between the branches can be achieved quickly; therefore, the unstable time becomes short. However, it is not able to make a large influence with only a limited increase in the gas phase due to the low momentum compared with the liquid phase.
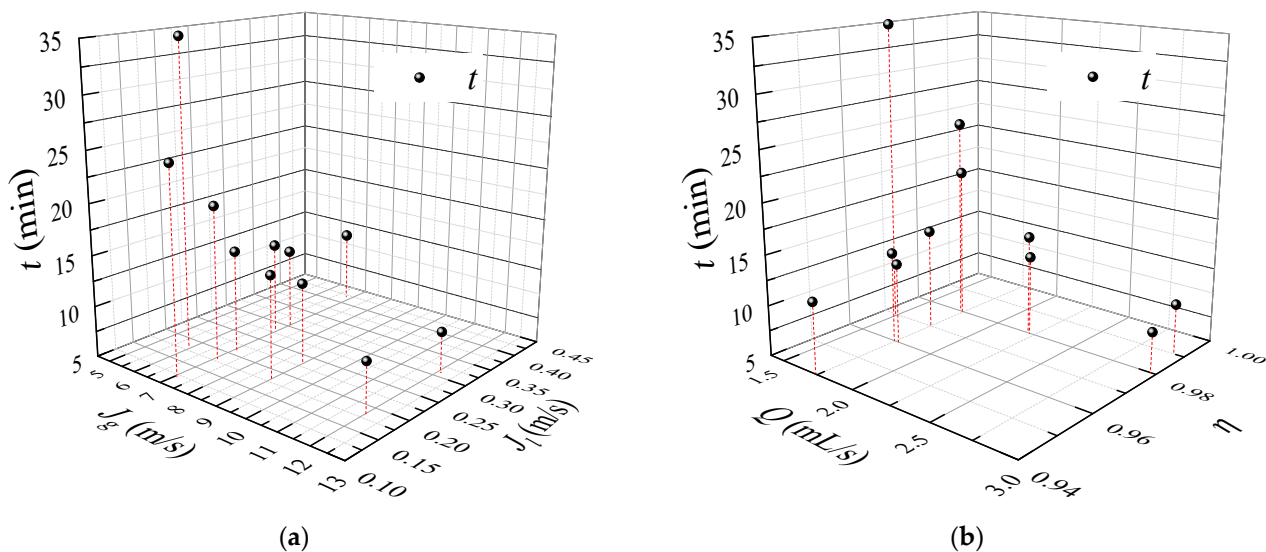

Figure 4. The effect of inlet conditions on the duration (t) of flow distribution varying. The black dots are the data of t and the red dotted lines indicate the inlet conditions for the data. (**a**) Effect of J_g & J_l; (**b**) Effect of Q & x_g.

3.3. Effect of Inlet Conditions on Phase Distribution

The distribution results of both liquid and gas at the stable region were plotted into four figures according to their series, as seen in Figure 5, in which the effect of the inlet liquid superficial velocity, gas superficial velocity, volume fraction of gas, and volume flow rate are shown in Figure 5a–d, respectively. Meanwhile, the corresponding typical flow structures in the header and branch channels in all cases are shown in Figure 6.
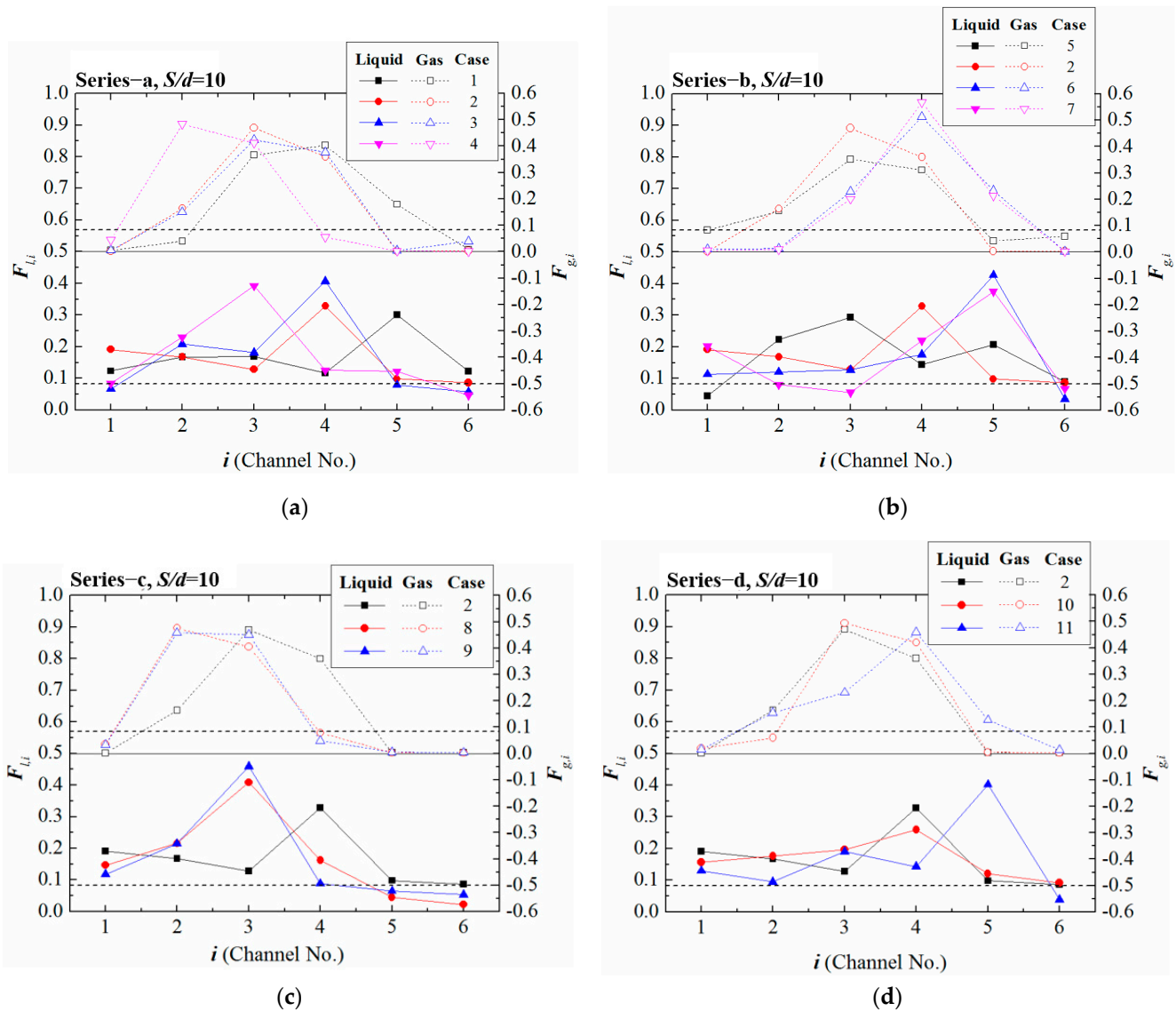

Figure 5. Phase distribution results under different inlet conditions. (**a**) Series-a; (**b**) Series-b; (**c**) Series-c; (**d**) Series-d.

As illustrated in Figure 5a, the liquid highly supplies channel #5 and moderately feeds the rest of the channels with a low inlet liquid superficial velocity, while it tends to feed the channels at the front part of the header with an increase in the liquid superficial velocity. The gas phase is mainly aspirated by the adjacent upstream channel of the one that is highly fed by the liquid phase. This agrees with the observed phenomenon shown in Figure 6a. The liquid column at the end of the header becomes longer with the increase in the inlet liquid superficial velocity, which facilitates the liquid to fill with the channels at the front part of the header. This is similar to the measured and observed results in series-c in that the liquid tends to be taken by the channels at the fore part of the header gradually with the inlet volume of gas decreasing, as seen in Figures 5c and 6c, whereas as the header gas

superficial velocity or volume flow rate increases, more liquid flows through the channels at the rear part of the header while the channels in the fore part of the header tend to be badly fed. This trend is consistent with the flow structures in the header observed, as seen in Figure 6b,d. Moreover, the distribution characteristics of the gas phase are the same as that in series-a and series-c.
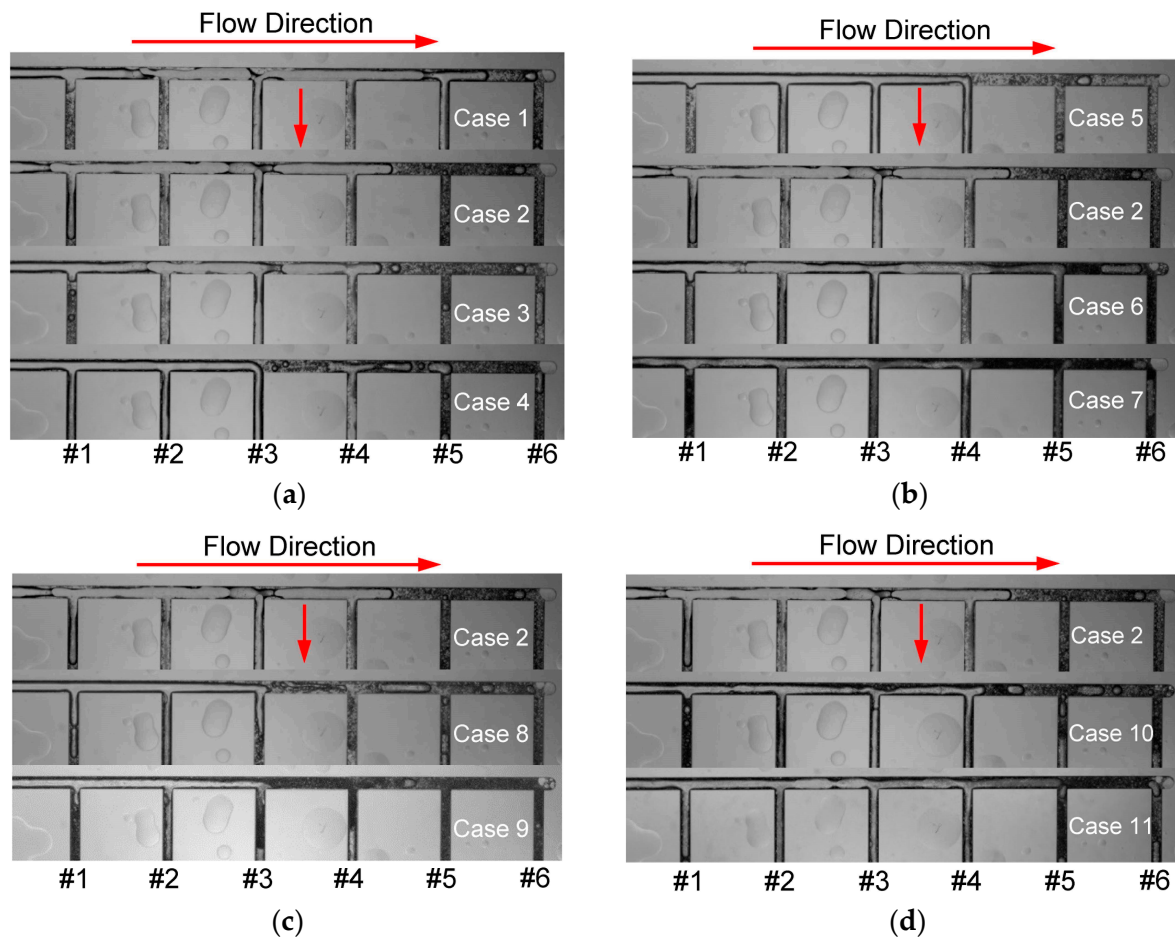

Figure 6. Typical flow structures in the header and branch channels under different inlet conditions. #1-6 are the channel numbers starting from the fluid inlet direction and the red arrows show the flow direction in the channels. (**a**) Series-a; (**b**) Series-b; (**c**) Series-c; (**d**) Series-d.

As mentioned in Wang et al. [34], the slug–annular flow was a compound flow pattern, which includes three sub-patterns, like a liquid bridge, wavy liquid film, and smooth liquid film, which are classified based on their different flow forms and momentums fluxes. In addition, the momentums of three sub-patterns could be sorted in descending order: liquid bridge > wavy liquid film > smooth liquid film, which had a significant effect on the liquid distribution, and the appearing probabilities of the three sub-patterns were related to the phase distribution. It is necessary to obtain the statistics of the appearing probabilities of sub-patterns. Therefore, the probability of the appearance of three sub-patterns in these experiments was also obtained (Figure 7). It is observed that increasing the appearing probabilities of the liquid bridge decreases the liquid mass fraction in the channels at the rear part of the header. This is because the liquid with a higher momentum prefers to stay in the header and enters the last few channels at the header while plenty of liquid blocks those channels and increases the pressure decrease, and then the liquid flows into the front channels gradually with the increasing appearing probabilities of the liquid bridge. Moreover, the wavy film has the same effect as the liquid bridge. Therefore, in series-d, the liquid tends to feed the channels at the rear part of the header when the inlet volume flow

rate increases, although the probability of the liquid bridge remains unchanged. Conversely, it is notable that each liquid bridge contains much more liquid than each wavy film, and the effect of the former is dominant when they go against each other. In addition, since the smooth film has the lowest momentum, most of the liquid film can be divided into the branch channels at the fore part of the header.
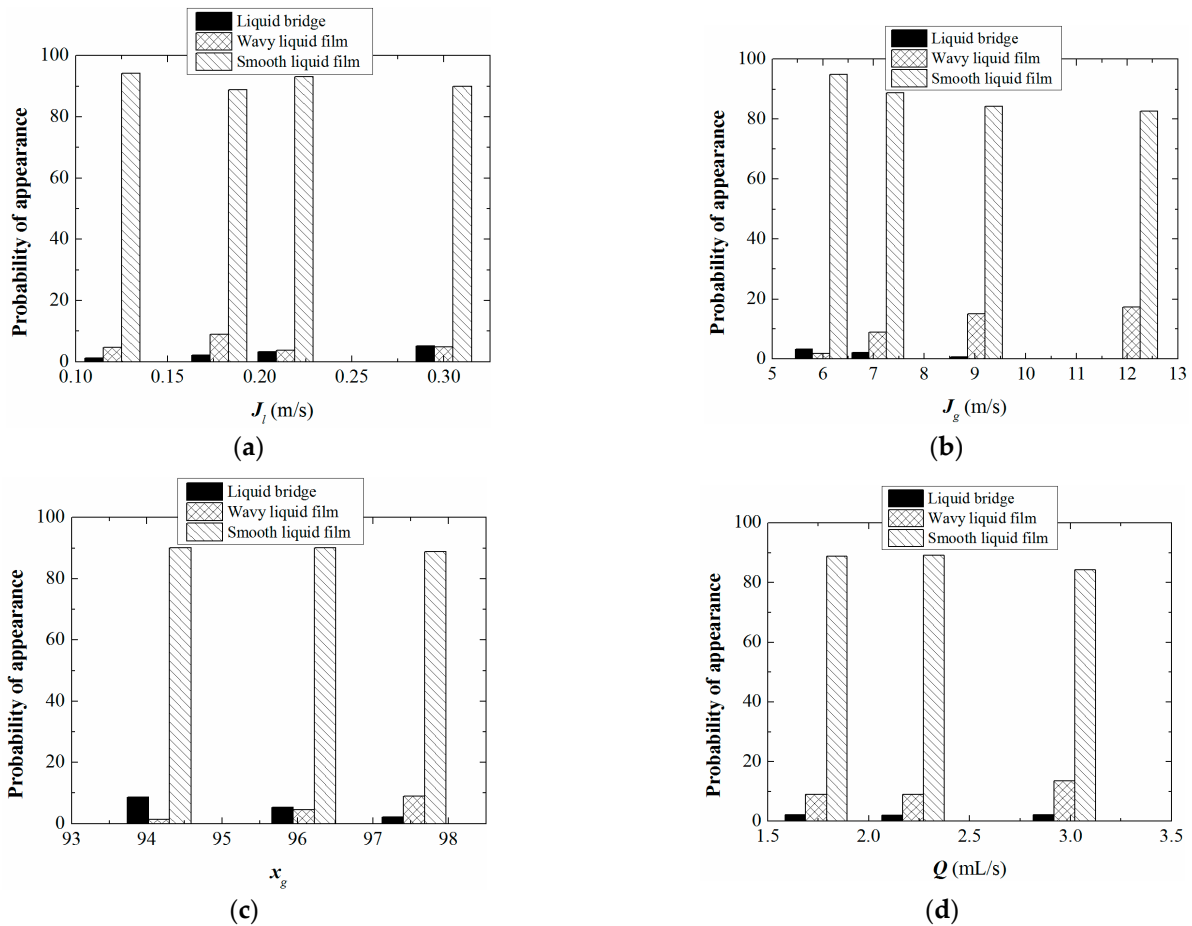

Figure 7. Probabilities of appearance of three sub-patterns under different inlet conditions. (**a**) Series-a; (**b**) Series-b; (**c**) Series-c; (**d**) Series-d.

3.4. Effect of the Branch Spacing on Phase Distribution

Typical flow structures in test sections with different branch spacings for case 4 and case 10 are illustrated in Figure 8 along with the liquid and gas distribution data. The findings from case 4 indicate a pronounced preference for the liquid phase to predominantly supply channels #1 and #2 when S/d equals 2. As the spacing-to-diameter ratio increases to 10, the liquid phase preferentially flows into channels #2 and #3, with a particular emphasis on channel #3. At a larger branch spacing of $S/d = 30$, the majority of the liquid is directed towards channel #5. Overall, it is observed that channels positioned towards the end of the header are increasingly favored by the liquid phase as the branch spacing widens. This is because the liquid pooling in the header is weaker with large spacing, as shown in Figure 8a, where there is more space between two channels to buffer a larger amount of liquid, thus preventing more channels at the fore part of the header from being blocked. For the gas phase, there is not much difference between test case $S/d = 10$ and $S/d = 30$, in which gas tends to feed the adjacent upstream channel of the one filled with the most liquid. The obvious distinction is that in the case of $S/d = 2$, the gas tends to feed channels #2 and #3 while badly supplying the other channels, and channel #2 is highly fed not only by the liquid but also by the gas. This means the end effect is predominant with small

branch spacing, and only the channels far away from the header end are easy to fill. In case 10, the liquid seems to be more homogenously distributed and the trend of the phase distribution when the branch spacing increases is similar to case 4 for both the liquid and gas. The distinct thing is that the mass flow fractions of the liquid and gas in the channels at the rear part are increased in this situation.
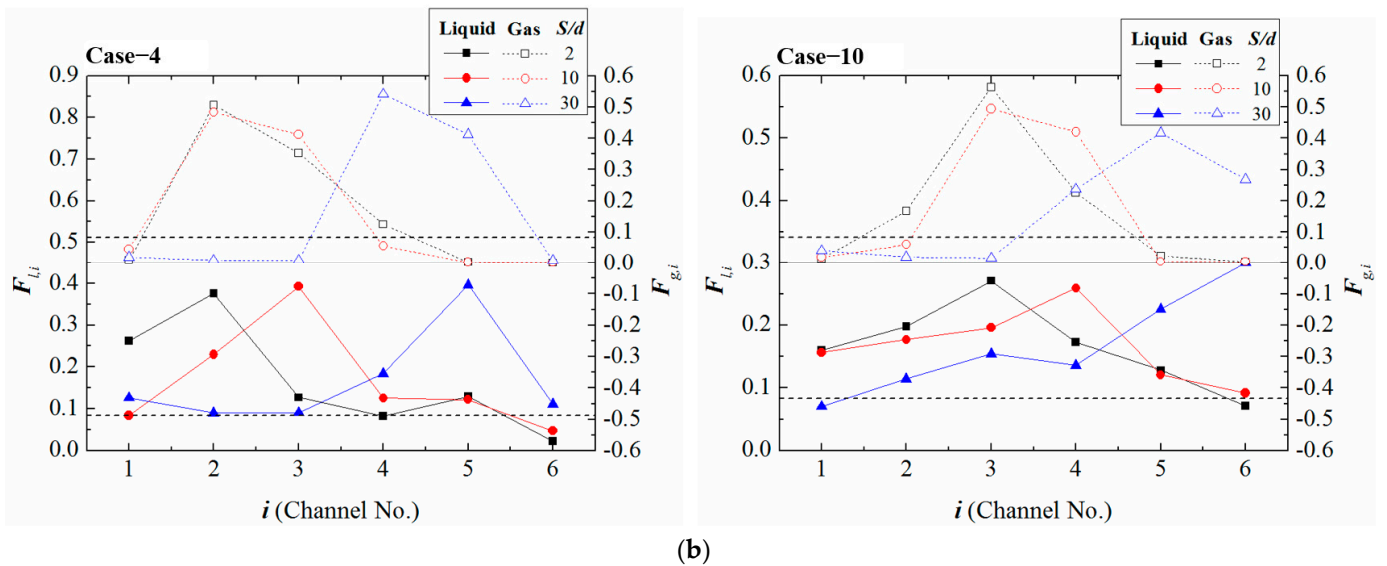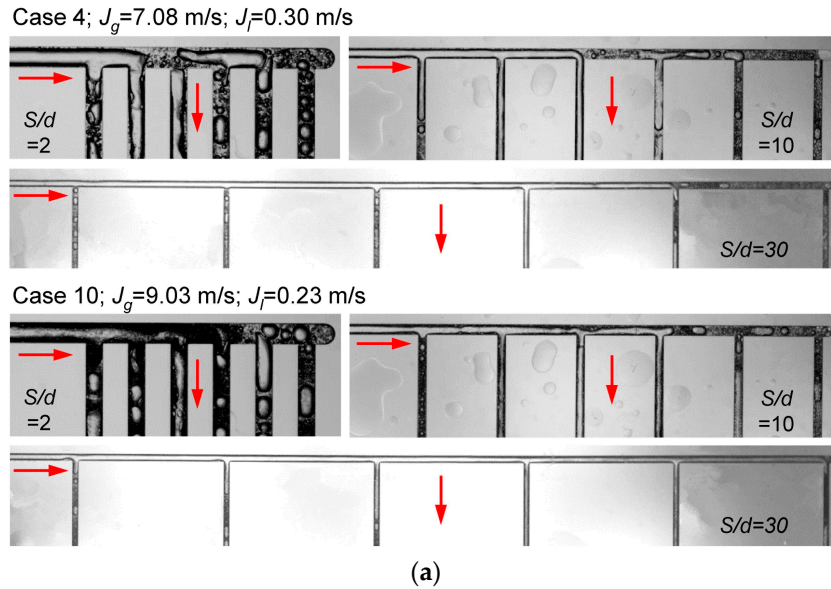

Figure 8. Typical flow pattern in header and branch channels and the corresponding liquid and gas distribution in case 4 and case 10. The red arrows show the flow direction in the channels. (**a**) Typical flow structures in header and branch channels; (**b**) Corresponding liquid and gas distribution.

3.5. Distribution Correlation

The research conducted by Watanabe et al. [35] and Byun and Kim [36], involving headers with diameters of 20 mm and 18 mm, respectively, suggests that the fraction of liquid diverted by a branch channel may be influenced by the gas Reynolds number just upstream in the header. Furthermore, the experimental findings from Zou and Hrnjak [37], who utilized headers of 15.44 mm and 14.94 mm, underscore the critical role of the inlet quality in determining the liquid distribution. The definitions of the parameters referenced by these scholars are depicted in Figure 9a. Calculations of the liquid fraction taken off
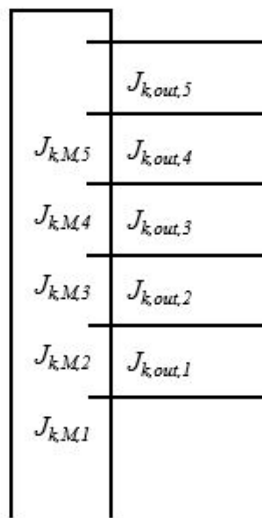
and the local dimensionless parameters for both the gas and liquid were derived from the experimental observations as
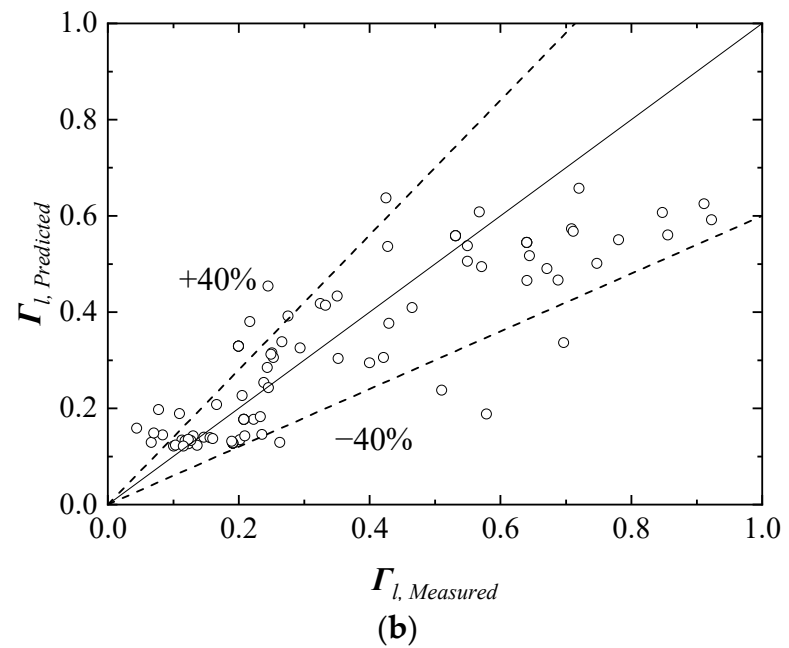
$$\Gamma_k = \frac{m_{k,out,i}}{m_{k,M,i}}, \tag{3}$$

$$Ca = \frac{\mu_l J_{l,M,i}}{\sigma_l}, \tag{4}$$

$$We_g = \frac{\rho_g J_{g,M,i}^2 D_h}{\sigma_g}, \tag{5}$$

$$Re_l = \frac{\rho_l J_{l,M,i} D_h}{\mu_l}. \tag{6}$$

Figure 9. (**a**) Header schematic and notations [38]; (**b**) Comparison between measured data and predictions.

In micro-channels (less than 1 mm), the interplay of surface tension and viscosity is crucial in influencing the flow dynamics. Within such contexts, the liquid Reynolds number at the immediate upstream position in the header plays a more pivotal role in determining the liquid distribution than does the gas Reynolds number for two-phase flows in micro-channels [38]. As highlighted by Hwang et al. [26] and Lee [39], increasing the branch spacing (*S*) allows for a greater fraction of the liquid phase to be diverted from the branch channels. They incorporated the influence of branch spacing into a flow split prediction model for parallel branches using a coefficient *C*. This coefficient is expected to approach unity for large inter-branch distances and decrease as the branch spacing narrows [27]. A novel correlation equation, derived from experimental data, is presented as follows:

$$\Gamma_l = 1.43 C \left(4.31 \Gamma_g + 1.25\right) Q^{0.13} x_g^{5.97} Ca^{0.34} We_g^{-0.08} Re_l^{-0.17}, \tag{7}$$

where

$$C = 1, \text{ for the first T} - \text{junction}, \tag{8}$$

$$C = \left(1 + \frac{d}{S}\right)^{-0.8}, \text{ for the downstream T} - \text{junctions}. \tag{9}$$

It is crucial to note that this correlation does not extend to the fraction of liquid captured by the terminal channel, as all the fluid reaching this channel's entry is inevitably absorbed, rendering the liquid take-off ratio (Γ_l) equal to 1 under all conditions. According to Equation (7), the liquid take-off ratio (Γ_l) escalates with an increase in the inlet gas volume fraction. A juxtaposition of empirical data against model predictions is depicted in Figure 9b, with 80% of the data points falling within a $\pm 40\%$ prediction band. Despite the correlation's limited precision, it surpasses existing empirical models for micro-parallel channels in terms of accuracy [20,37,40]. Nonetheless, there remains significant scope for refining this distribution correlation in future research endeavors.

4. Conclusions

An experimental investigation was conducted on the distribution of gas–liquid two-phase slug–annular flow across six parallel micro-channels. This study focused on examining the impact of the inlet conditions and branch spacing on the dynamics of the two-phase flow through a comprehensive series of experiments.

1. The phase distribution is highly dependent on the inlet conditions. An increase in the liquid superficial velocity can facilitate the liquid phase to flow into channels at the fore part of the header, while the channels at the rear part of the header are more supplied with liquid as the gas superficial velocity, volume fraction of gas, and volume flow rate increase. In addition, the trend of the gas distribution changing with that of the liquid and the gas phases is always mainly aspirated by the adjacent upstream channel of the one that is highly fed by the liquid phase.
2. The distribution of slug–annular flow is the lack of stability and the unstable time regularly changes. With an increase in the inlet liquid superficial velocity, the gas superficial velocity, and the volume flow rate, it takes less time for the distribution to be stable, whereas an increase in the volume fraction of gas can extend the stabilization time.
3. As for the effect of the branch spacing, the results show that the channels at the rear part of the header tend to be highly supplied by both the liquid and gas phases with an increase in the branch spacing.
4. An empirical correlation relating the liquid and gas taken off the same branch was obtained using two inlet parameters and three non-dimensional numbers. The comparisons between the measured data and the predicted data show relatively good agreement.

The present study may provide some guidance for the application of slug–annular flow in multi-parallel channels. The observed flow patterns in the transparent test sections can be helpful in understanding the distribution of the two-phase flow and building the theoretical modeling of slug–annular flow.

Author Contributions: Conceptualization, S.W. and Y.L.; methodology, Y.L.; validation, Y.L. and S.J.; investigation, Y.L.; resources, S.W.; data curation, Y.L. and S.J.; writing—original draft preparation, Y.L.; writing—review and editing, S.W.; visualization, Y.L.; supervision, S.W.; funding acquisition, S.W. and Y.L. All authors have read and agreed to the published version of the manuscript.

Data Availability Statement: The data that support the findings of this study are available from the corresponding author upon reasonable request.

Conflicts of Interest: The authors declare no conflicts of interest.

Nomenclature and Subscripts

Γ	Phase take-off ratio		S	Distance between adjacent channels, mm
μ	Viscosity, cP		t	Time, min
ρ	Density, kg/m^3		We	Weber number
σ	Surface tension coefficient of the liquid, mN/m		x	Volume fraction
Ca	Capillary number		g	Gas phase
d	Hydraulic diameter of the branch channel, mm		h	Hydraulic
D	Hydraulic diameter of the header, mm		i	Number of channels
F	Phase take-off fraction		in	At the inlet
J	Superficial velocity, m/s		k	l or g
m	Mass flow rate, kg/s		l	Liquid phase
Q	Volume flow rate, mL/s		M	Main tube (header)
Re	Reynolds number of the gas at the inlet		out	Out from the header

References

1. Elvira, K.S.; Casadevall i Solvas, X.; Wootton, R.C.R.; deMello, A.J. The past, present and potential for microfluidic reactor technology in chemical synthesis. *Nat. Chem.* **2013**, *5*, 905–915. [CrossRef] [PubMed]
2. Van Oevelen, T.; Weibel, J.A.; Garimella, S.V. The effect of lateral thermal coupling between parallel microchannels on two-phase flow distribution. *Int. J. Heat Mass Tran.* **2018**, *124*, 769–781. [CrossRef]
3. Hong, S.; Li, C.; Dang, C.; Song, M.; Sakamoto, H. Experimental research on cooling performances of radial expanding-channeled heat sinks applied for multiple heat sources. *Appl. Therm. Eng.* **2024**, *237*, 121789. [CrossRef]
4. Triplett, K.A.; Ghiaasiaan, S.M.; Abdel-Khalik, S.I.; Sadowski, D.L. Gas–liquid two-phase flow in microchannels Part I: Two-phase flow patterns. *Int. J. Multiph. Flow* **1999**, *25*, 377–394. [CrossRef]
5. Hajmohammadi, M.R.; Alipour, P.; Parsa, H. Microfluidic effects on the heat transfer enhancement and optimal design of microchannels heat sinks. *Int. J. Heat Mass Tran.* **2018**, *126*, 808–815. [CrossRef]
6. Lalot, S.; Florent, P.; Lang, S.K.; Bergles, A.E. Flow maldistribution in heat exchangers. *Appl. Therm. Eng.* **1999**, *19*, 847–863. [CrossRef]
7. Rao Bobbili, P.; Sunden, B.; Das, S.K. Thermal analysis of plate condensers in presence of flow maldistribution. *Int. J. Heat Mass Tran.* **2006**, *49*, 4966–4977. [CrossRef]
8. Wu, X.M.; Webb, R.L. Thermal and hydraulic analysis of a brazed aluminum evaporator. *Appl. Therm. Eng.* **2002**, *22*, 1369–1390. [CrossRef]
9. Dario, E.R.; Tadrist, L.; Passos, J.C. Review on two-phase flow distribution in parallel channels with macro and micro hydraulic diameters: Main results, analyses, trends. *Appl. Therm. Eng.* **2013**, *59*, 316–335. [CrossRef]
10. Marchitto, A.; Devia, F.; Fossa, M.; Guglielmini, G.; Schenone, C. Experiments on two-phase flow distribution inside parallel channels of compact heat exchangers. *Int. J. Multiph. Flow* **2008**, *34*, 128–144. [CrossRef]
11. Osakabe, M.; Hamada, T.; Horiki, S. Water flow distribution in horizontal header contaminated with bubbles. *Int. J. Multiph. Flow* **1999**, *25*, 827–840. [CrossRef]
12. Kim, N.H.; Sin, T.R. Two-phase flow distribution of air–water annular flow in a parallel flow heat exchanger. *Int. J. Multiph. Flow* **2006**, *32*, 1340–1353. [CrossRef]
13. Ahmad, M.; Berthoud, G.; Mercier, P. General characteristics of two-phase flow distribution in a compact heat exchanger. *Int. J. Heat Mass Tran.* **2009**, *52*, 442–450. [CrossRef]
14. Dario, E.R.; Tadrist, L.; Oliveira, J.L.G.; Passos, J.C. Measuring maldistribution of two-phase flows in multi-parallel microchannels. *Appl. Therm. Eng.* **2015**, *91*, 924–937. [CrossRef]
15. Liu, Y.; Sun, W.; Wu, W.; Wang, S. Gas-liquid two-phase flow distribution in parallel micro-channels with different header and channels' orientations. *Int. J. Heat Mass Tran.* **2017**, *112*, 767–778. [CrossRef]
16. Zhang, Q.; Hrnjak, P.; Newell, T. An Experimental Investigation of R134a Flow Distribution in Horizontal Microchannel Manifolds. In *TR-223*; Air Conditioning and Refrigeration Center, University of Illinois at Urbana-Champaign: Champaign, IL, USA, 2003.
17. Kim, N.H.; Kim, D.Y.; Byun, H.W. Effect of inlet configuration on the refrigerant distribution in a parallel flow minichannel heat exchanger. *Int. J. Refrig.* **2011**, *34*, 1209–1221. [CrossRef]
18. Kim, N.H.; Kim, D.Y.; Cho, J.P.; Kim, J.O.; Park, T.K. Effect of flow inlet or outlet direction on air-water two-phase distribution in a parallel flow heat exchanger header. *Int. J. Air-Cond. Refrig.* **2008**, *16*, 37–43.
19. Chen, J.; Wang, S.; Cheng, S. Experimental investigation of two-phase distribution in parallel micro-T channels under adiabatic condition. *Chem. Eng. Sci.* **2012**, *84*, 706–717. [CrossRef]
20. Zou, Y.; Hrnjak, P.S. Effects of fluid properties on two-phase flow and refrigerant distribution in the vertical header of a reversible microchannel heat exchanger—Comparing R245fa, R134a, R410A, and R32. *Appl. Therm. Eng.* **2014**, *70*, 966–976. [CrossRef]
21. Horiki, S.; Nakamura, T.; Osakabe, M. Thin flow header to distribute feed water for compact heat exchanger. *Exp. Therm. Fluid Sci.* **2004**, *28*, 201–207. [CrossRef]

22. Vist, S.; Pettersen, J. Two-phase flow distribution in compact heat exchanger manifolds. *Exp. Therm. Fluid Sci.* **2004**, *28*, 209–215. [CrossRef]
23. Lee, J.K.; Lee, S.Y. Distribution of two-phase annular flow at header–channel junctions. *Exp. Therm. Fluid Sci.* **2004**, *28*, 217–222. [CrossRef]
24. Kim, N.H.; Han, S.P. Distribution of air–water annular flow in a header of a parallel flow heat exchanger. *Int. J. Heat Mass Tran.* **2008**, *51*, 977–992. [CrossRef]
25. Marchitto, A.; Fossa, M.; Guglielmini, G. Phase split in parallel vertical channels in presence of a variable depth protrusion header. *Exp. Therm. Fluid Sci.* **2016**, *74*, 257–264. [CrossRef]
26. Hwang, S.T.; Soliman, H.M.; Lahe, R.T., Jr. Phase separation in dividing two-phase flows. *Int. J. Multiph. Flow* **1988**, *14*, 439–458. [CrossRef]
27. Lee, J.K. Branching of two-phase flow from a vertical header to horizontal parallel channels. *J. Mech. Sci. Technol.* **2010**, *23*, 1628–1636. [CrossRef]
28. Yin, Y.; Zhu, C.; Guo, R.; Fu, T.; Ma, Y. Gas-liquid two-phase flow in a square microchannel with chemical mass transfer: Flow pattern, void fraction and frictional pressure drop. *Int. J. Heat Mass Tran.* **2018**, *127*, 484–496. [CrossRef]
29. Fouilland, T.S.; Fletcher, D.F.; Haynes, B.S. Film and slug behaviour in intermittent slug–annular microchannel flows. *Chem. Eng. Sci.* **2010**, *65*, 5344–5355. [CrossRef]
30. Thiangtham, P.; Keepaiboon, C.; Kiatpachai, P.; Asirvatham, L.G.; Mahian, O.; Dalkilic, A.S.; Wongwises, S. An experimental study on two-phase flow patterns and heat transfer characteristics during boiling of R134a flowing through a multi-microchannel heat sink. *Int. J. Heat Mass Tran.* **2016**, *98*, 390–400. [CrossRef]
31. Chung, P.M.Y.; Kawaji, M. The effect of channel diameter on adiabatic two-phase flow characteristics in microchannels. *Int. J. Multiph. Flow* **2004**, *30*, 735–761. [CrossRef]
32. Thulasidas, T.C.; Abraham, M.A.; Cerro, R.L. Flow patterns in liquid slugs during bubble-train flow inside capillaries. *Chem. Eng. Sci.* **1997**, *52*, 2947–2962.
33. Liu, Y.; Wang, S. Distribution of gas-liquid two-phase slug flow in parallel micro-channels with different branch spacing. *Int.J. Heat Mass Tran.* **2019**, *132*, 606–617. [CrossRef]
34. Wang, S.; He, K.; Huang, J. Phase splitting of a slug–annular flow at a horizontal micro-T-junction. *Int. J. Heat Mass Tran.* **2011**, *54*, 589–596. [CrossRef]
35. Watanabe, M.; Katsuta, M.; Nagata, K. General characteristics of two-phase flow distribution in a multipass tube. *Heat Transf. Jpn. Res.* **1995**, *24*, 32–44.
36. Byun, H.W.; Kim, N.H. Refrigerant distribution in a parallel flow heat exchanger having vertical headers and heated horizontal tubes. *Exp. Therm. Fluid Sci.* **2011**, *35*, 920–932. [CrossRef]
37. Zou, Y.; Hrnjak, P.S. Experiment and visualization on R134a upward flow in the vertical header of microchannel heat exchanger and its effect on distribution. *Int. J. Heat Mass Transf.* **2013**, *62*, 124–134. [CrossRef]
38. Chen, J.; Wang, S.; Zhang, X.; Ke, H.; Li, X. Experimental investigation of two-phase slug flow splitting at a micro impacting T-junction. *Int. J. Heat Mass Tran.* **2015**, *81*, 939–948. [CrossRef]
39. Lee, J.K. Two-phase flow behavior inside a header connected to multiple parallel channels. *Exp. Therm. Fluid Sci.* **2009**, *33*, 195–202. [CrossRef]
40. Kim, N.-H.; Lee, E.-J.; Byun, H.-W. Two-phase refrigerant distribution in a parallel flow minichannel heat exchanger having horizontal headers. *Int. J. Heat Mass Transf.* **2012**, *55*, 7747–7759. [CrossRef]